11th ANKARA INTERNATIONAL AEROSPACE CONFERENCE **AIAC-2021-112**
8-10 September 2021 - METU, Ankara TURKEY

Global linear parameter varying (LPV) model development for fighter aircraft

Murat Millidere[1]
Middle East Technical University (METU),
Ankara, Turkey

Samet Uslu[2], Tolga Yigit[3] and Himmet Arın Ozkul[4]
Turkish Aerospace (TA)
Ankara, Turkey

ABSTRACT

An air vehicle has highly nonlinear and complicated dynamics, which means that it is difficult to accurately model an air vehicle using linear equations. In order to design a controller for an air vehicle, the dynamic behavior of the aircraft must be well understood in varying flight conditions. Nevertheless, the dynamics are ordinarily obtained in a single flight condition, and controllers are often designed to respond to a specific flight condition. In order to represent the dynamics of air vehicle for the full flight envelope, Linear Parameter Varying (LPV) modeling approach is used. There are several methods for LPV modeling. The aim of this paper is to compare effectiveness of two methods in LPV modeling which are "Jacobian Linearization" and "Stitching Model" by comparing time responses with nonlinear model. The presented methods enable the simulation of the air vehicle as well as predicting its dynamic properties across the considered part of the flight envelope. Additionally, the comparison is expected to present advantages and disadvantages of the methods as well as presenting the results in the considered part of the flight envelope.

INTRODUCTION

In order to design a controller for an air vehicle, it is needed to represent the dynamics of air vehicle over full flight envelope. Nevertheless, the dynamics are ordinarily obtained in single flight condition, and controllers are often designed to respond to a specific flight condition. Then, controller parameters are scheduled in order to be applied for full flight envelope. Another way to be applied for full flight envelope is to obtain LPV models. A family of local linear time-invariant (LTI) models at different points and trim data, which covers a significant part of the flight envelope, is combined in order to obtain a LPV model. In other words, LPV modeling methods lean on the idea that a global model is comprised of infinite number of local linearized models. If local linearized models are interpolated within the flight envelope, these will result in a full flight envelope model. LPV models are a key step in applying LPV control synthesis which guarantee a level of stability and robustness for the closed loop [1]. LPV modelling is closely related to gain-scheduling control. LPV modelling is not frequently considered as an independent research topic and most of the available literature is only

[1] PhD Candidate, Email: murat.millidere@gmail.com
[2] Flight Control Algorithm Design, Email: samet.uslu@tai.com.tr
[3] Flight Control Algorithm Design, Email: tolga.yigit@tai.com.tr
[4] Flight Control Algorithm Design, Email: himmetarin.ozkul@tai.com.tr

concerned with LPV control for a given LPV model. There are several ways of LPV modeling such as Jacobian Linearization, State Transformation, Function Substitution and Model Stitching.

This paper presents a comparison between two LPV modelling approaches for a fighter aircraft. Methods presented in the paper obtain quasi-LPV model. A quasi-LPV model (qLPV), which is a particular case of an LPV model that is characterized by having a subset of the scheduling parameters belong to state-space of the system. Creating a qLPV model involves two steps: firstly, local linear models are obtained; secondly, a set of interpolating functions are determined to combine these models into a global LPV model. One of the methods which will be presented in the paper is Jacobian Linearization. The Jacobian Linearization approach is the most widespread methodology to linearize nonlinear systems. It is also applicable to the widest class of nonlinear systems since it is valid for any nonlinear system that can be linearized at its equilibrium (trim) points. The main concept of this method is to use first order Taylor's expansion of the nonlinear model with respect to a trim point [3]. Second of the methods which will be presented in the paper is Stitching Model which provides a continuous simulation that is grounded on several discrete linear models and trim data. The model stitching simulation architecture can be used on any physical model that can be accurately represented using state equations, where needed, flight test data can be acquired. Discrete linear models and trim data, which represent models, are tabulated and taken into account with nonlinear effects to produce a continuous simulation model.

The contribution of this study will be to compare two methods in order to determine effectiveness of methods using the example of an existing fighter aircraft. Starting from trim analyses in which Newton Raphson approach [2] is used, the dynamics of the air vehicle covering a range of different flight conditions are identified by using both methods.

Local LTI models and trim data are obtained in 12 different trim points with combination of two different altitude (10000 ft and 25000 ft) and 6 different speed settings (0.2 Mach to 0.6 Mach) from a nonlinear fighter aircraft simulation model [6]. A discussion of advantages and disadvantages of aforementioned LPV modeling methods will be presented. In order to compare the efficiency of these methods, open loop time responses of the LPV models for each LPV modeling methods are obtained and compared to the nonlinear aircraft responses using the off-nominal points that were not used to obtain the LPV model.

METHOD

1. Jacobian Linearization

The most widely used technique for obtaining LPV models of nonlinear systems is the Jacobian linearization approach. It also applies to the broadest category of nonlinear systems, since it is true for any nonlinear system that can be linearized at its equilibrium points. It can be used to build an LPV system out of a family of plants that have been linearized with respect to a set of equilibrium points that represent the desired flight envelope. The model after that provides a low-order description of the nonlinear system dynamics around these equilibrium points. The basis of this method is to use a first order Taylor series expansion of the nonlinear model, equation (1), with respect to a trim point shown in equation (2).

$$\delta_{f_i} = \Delta_z f \cdot \delta_z + \Delta_w f \cdot \delta_w + \Delta_u f \cdot \delta_u \quad (1)$$
$$= \Delta_z f(z - z_{eq}) + \Delta_w f(w - w_{eq}) + \Delta_u f(u - u_{eq})$$

$$\delta_{f_1} = f_1(z_1 w_1 u) - f_1(z_1 w_1 u)|_{eq} \quad (2)$$

The term $\Delta_z f$ as shown above remarks derivative of function f with respect to z. If equations are formed in state-space form, shown in (3).

$$\begin{bmatrix} \dot{\delta}_z \\ \dot{\delta}_w \end{bmatrix} = \begin{bmatrix} \Delta_z f_1 & \Delta_w f_1 \\ \Delta_z f_2 & \Delta_w f_2 \end{bmatrix}_{eq} \begin{bmatrix} \delta_z \\ \delta_w \end{bmatrix} + \begin{bmatrix} \Delta_u f_1 \\ \Delta_u f_2 \end{bmatrix}_{eq} [\delta_u] \tag{3}$$

It is easy to verify that the trim values, and all the elements in the state-space matrices depend on the scheduling variables and hence the model is quasi-LPV [3]. A more detailed theoretical derivation of a Jacobian model is given in [7].

The approximated model could lead to divergent behavior, with respect to large nonlinear inputs because of being a first order approximation. The local model could be calculated by utilizing higher-order terms in the Taylor series, but these results are intractable, making them infeasible.

2. Model Stitching

The term model stitching refers to the technique of combining or "stitching" together a collection of linear state-space models for discrete flight conditions, with corresponding trim data, into one continuous, full-envelope flight dynamics simulation model [4]. In this method, lookup tables as a function of airspeed are established with using stability and control derivatives which are provided for each discrete linearized model. This method is also in the class of qLPV as well as Jacobian Linearization. The linear stability and control derivatives, as well as trim data, are scheduled in the resulting model, but equations of motion and gravitational force equations are implemented nonlinearly. In other words, this method provides us a linear flight simulation model with time-varying aerodynamics.

As a starting point, model is stitched over the trim values. So, perturbation terms will be added to the state space representation in Equation (4).

$$\begin{aligned} \dot{\vec{x}} &= A\vec{x} + B\vec{u} \\ \dot{\overrightarrow{x_0}} + \dot{\overrightarrow{\Delta x}} &= A\left(\overrightarrow{x_0} + \overrightarrow{\Delta x}\right) + B\left(\overrightarrow{u_0} + \overrightarrow{\Delta u}\right) \end{aligned} \tag{4}$$

where $\overrightarrow{x_0}$ and $\overrightarrow{u_0}$ are the vectors of trim aircraft states and trim controls and $\overrightarrow{\Delta x}$ and $\overrightarrow{\Delta u}$ represent the state perturbation vector and control perturbation vector, respectively.

This section provides a walkthrough of the top-level model stitching simulation architecture. Figure 1 shows a top-level schematic of the model stitching architecture, illustrating all the key simulation elements.

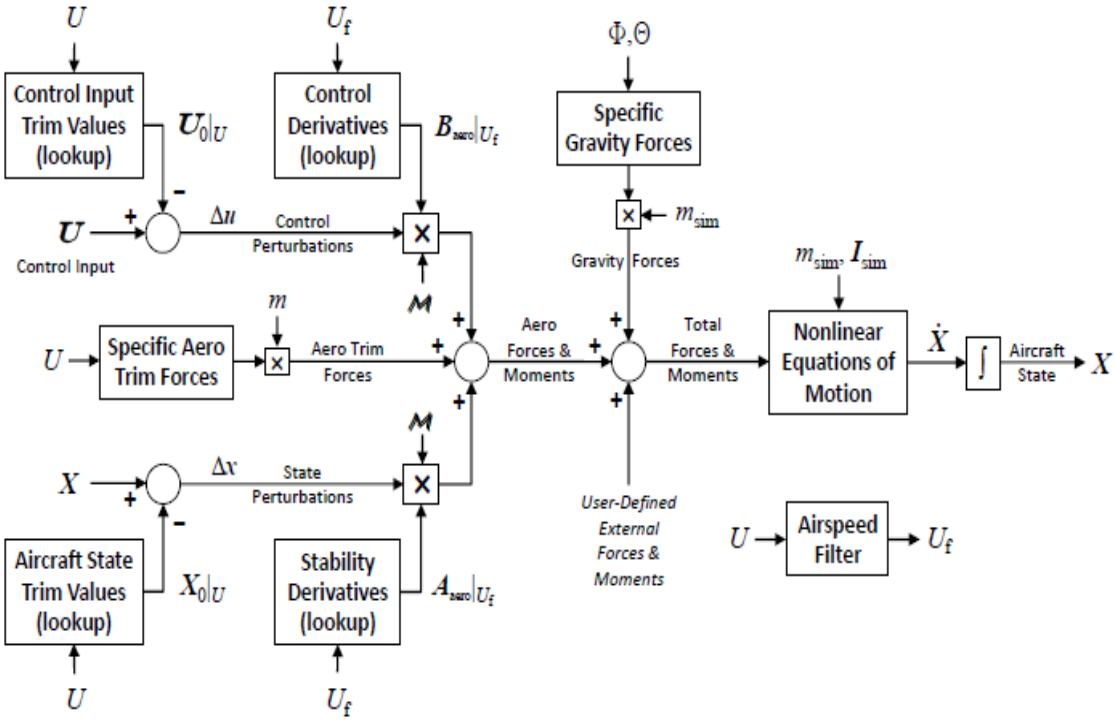

Figure 1 Model stitching simulation architecture - top level schematic

There are control derivatives and stability derivatives lookup tables in Figure 1. In order to derive them, small perturbation is applied to equations of motion resulting with Equation (5).

$$A = \begin{bmatrix} \tilde{X}_u & \tilde{X}_v & \tilde{X}_w & \tilde{X}_p & \tilde{X}_q - w_0 & \tilde{X}_r + v_0 & 0 & -gc_{(\theta_0)} \\ \tilde{Y}_u & \tilde{Y}_v & \tilde{Y}_w & \tilde{Y}_p + w_0 & \tilde{Y}_q & \tilde{Y}_r - u_0 & gc_{(\phi_0)}c_{(\theta_0)} & -gs_{(\phi_0)}s_{(\theta_0)} \\ \tilde{Z}_u & \tilde{Z}_v & \tilde{Z}_w & \tilde{Z}_p - v_0 & \tilde{Z}_q + u_0 & \tilde{Z}_r & -gs_{(\phi_0)}c_{(\theta_0)} & -gc_{(\phi_0)}s_{(\theta_0)} \\ l'_u & l'_v & l'_w & l'_p & l'_p & l'_p & 0 & 0 \\ m'_u & m'_v & m'_w & m'_p & m'_q & m'_r & 0 & 0 \\ n'_u & n'_v & n'_w & n'_p & n'_q & n'_r & 0 & 0 \\ 0 & 0 & 0 & 1 & s_{(\phi_0)}t_{(\theta_0)} & c_{(\phi_0)}t_{(\theta_0)} & 0 & 0 \\ 0 & 0 & 0 & 0 & c_{(\phi_0)} & -s_{(\phi_0)} & 0 & 0 \end{bmatrix} \quad (5)$$

$$B = \begin{bmatrix} \tilde{X}_{\delta_t} & \tilde{X}_{\delta_e} & \tilde{X}_{\delta_a} & \tilde{X}_{\delta_r} \\ \tilde{Y}_{\delta_t} & \tilde{Y}_{\delta_e} & \tilde{Y}_{\delta_a} & \tilde{Y}_{\delta_r} \\ \tilde{Z}_{\delta_t} & \tilde{Z}_{\delta_e} & \tilde{Z}_{\delta_a} & \tilde{Z}_{\delta_r} \\ l'_{\delta_t} & l'_{\delta_e} & l'_{\delta_a} & l'_{\delta_r} \\ m'_{\delta_t} & m'_{\delta_e} & m'_{\delta_a} & m'_{\delta_r} \\ n'_{\delta_t} & n'_{\delta_e} & n'_{\delta_a} & n'_{\delta_r} \\ 0 & 0 & 0 & 0 \\ 0 & 0 & 0 & 0 \end{bmatrix}$$

Note that the A matrix includes gravity terms (e.g., $-gc_{(\theta_0)}$), Coriolis terms (e.g., $-w_0$), and kinematic terms (e.g., $s_{(\phi_0)}t_{(\theta_0)}$). For use in the model stitching, we introduce variations of A and B matrices that contain only the aerodynamic/propulsive dimensional stability and control derivatives; they do not contain gravity, Coriolis, or kinematic terms, and neither Euler angle states (ϕ, θ). Gravity is later incorporated using a nonlinear representation of the gravitational

forces and, Coriolis and kinematics are incorporated within the nonlinear equations of motion as seen in Figure 1. These aerodynamic/propulsive isolated matrices are denoted $A_{a/p}$ and $B_{a/p}$, and are given in equation (6).

$$A_{a/p} = \begin{bmatrix} \tilde{X}_u & \tilde{X}_v & \tilde{X}_w & \tilde{X}_p & \tilde{X}_q & \tilde{X}_r \\ \tilde{Y}_u & \tilde{Y}_v & \tilde{Y}_w & \tilde{Y}_p & \tilde{Y}_q & \tilde{Y}_r \\ \tilde{Z}_u & \tilde{Z}_v & \tilde{Z}_w & \tilde{Z}_p & \tilde{Z}_q & \tilde{Z}_r \\ l'_u & l'_v & l'_w & l'_p & l'_p & l'_r \\ m'_u & m'_v & m'_w & m'_p & m'_q & m'_r \\ n'_u & n'_v & n'_w & n'_p & n'_q & n'_r \end{bmatrix}$$

$$B_{a/p} = \begin{bmatrix} \tilde{X}_{\delta_t} & \tilde{X}_{\delta_e} & \tilde{X}_{\delta_a} & \tilde{X}_{\delta_r} \\ \tilde{Y}_{\delta_t} & \tilde{Y}_{\delta_e} & \tilde{Y}_{\delta_a} & \tilde{Y}_{\delta_r} \\ \tilde{Z}_{\delta_t} & \tilde{Z}_{\delta_e} & \tilde{Z}_{\delta_a} & \tilde{Z}_{\delta_r} \\ l'_{\delta_t} & l'_{\delta_e} & l'_{\delta_a} & l'_{\delta_r} \\ m'_{\delta_t} & m'_{\delta_e} & m'_{\delta_a} & m'_{\delta_r} \\ n'_{\delta_t} & n'_{\delta_e} & n'_{\delta_a} & n'_{\delta_r} \end{bmatrix} \quad (6)$$

Table look-ups are performed on the $A_{a/p}$ and $B_{a/p}$ matrices to find the dimensional stability and control derivatives at the current, x-body airspeed u. X-body airspeed u is used for look-up of derivatives only and is implemented to ensure that the derivative values remain constant for short-term motion, thereby retaining accurate dynamic responses at the discrete trim points.

Now we introduce a dimensional mass matrix $\mathcal{M}$ comprised of the aircraft mass (*m*) and inertia tensor ($\check{I}_B^B$) as shown in equation (7).

$$\mathcal{M} = \begin{bmatrix} m & & & & & \\ & m & & & & \\ & & m & & & \\ & & & I_{XX} & & -I_{XZ} \\ & & & & I_{YY} & \\ & & & -I_{XZ} & & I_{ZZ} \end{bmatrix} \quad (7)$$

Multiplying the mass matrix $\mathcal{M}$ into the matrix of aerodynamic/propulsive stability derivatives and the state perturbation vector $\overrightarrow{\mathbf{\Delta}x}$ yields a vector of aerodynamic dimensional perturbation forces and moments. Likewise, multiplying the mass matrix into the matrix of aerodynamic control derivatives and the control perturbation vector $\overrightarrow{\mathbf{\Delta}u}$ produces a vector of dimensional perturbation forces and moments. The sum of both vectors yields the complete aerodynamic dimensional perturbation forces and moments as shown in equation (8).

$$\begin{bmatrix} \Delta X \\ \Delta Y \\ \Delta Z \\ \Delta l \\ \Delta m \\ \Delta n \end{bmatrix} = \mathcal{M} A_{a/p} \begin{bmatrix} \Delta u \\ \Delta v \\ \Delta w \\ \Delta p \\ \Delta q \\ \Delta r \end{bmatrix} + \mathcal{M} B_{a/p} \begin{bmatrix} \Delta \delta_t \\ \Delta \delta_e \\ \Delta \delta_a \\ \Delta \delta_r \end{bmatrix} \quad (8)$$

where

$$\mathcal{M}A_{a/p} = \begin{bmatrix} X_u & X_v & X_w & X_p & X_q & X_r \\ Y_u & Y_v & Y_w & Y_p & Y_q & Y_r \\ Z_u & Z_v & Z_w & Z_p & Z_q & Z_r \\ l_u & l_v & l_w & l_p & l_q & l_r \\ m_u & m_v & m_w & m_p & m_q & m_r \\ n_u & n_v & n_w & n_p & n_q & n_r \end{bmatrix}$$

$$\mathcal{M}B_{a/p} = \begin{bmatrix} X_{\delta_t} & X_{\delta_e} & X_{\delta_a} & X_{\delta_r} \\ Y_{\delta_t} & Y_{\delta_e} & Y_{\delta_a} & Y_{\delta_r} \\ Z_{\delta_t} & Z_{\delta_e} & Z_{\delta_a} & Z_{\delta_r} \\ l_{\delta_t} & l_{\delta_e} & l_{\delta_a} & l_{\delta_r} \\ m_{\delta_t} & m_{\delta_e} & m_{\delta_a} & m_{\delta_r} \\ n_{\delta_t} & n_{\delta_e} & n_{\delta_a} & n_{\delta_r} \end{bmatrix} \quad (9)$$

In equation (8), in the complete aerodynamic/propulsion dimensional perturbation forces and moments, indices of row 1-3 is attributed to perturbation force vector, and indices of 4-6 is attributed to perturbation moment vector as shown in equation (10). This expression is shown in Figure 2.

$$\overrightarrow{\Delta f_{a,p}} = \begin{bmatrix} \Delta X \\ \Delta Y \\ \Delta Z \end{bmatrix}, \overrightarrow{\Delta m_{B_{a,p}}} = \begin{bmatrix} \Delta l \\ \Delta m \\ \Delta n \end{bmatrix}, \quad (10)$$

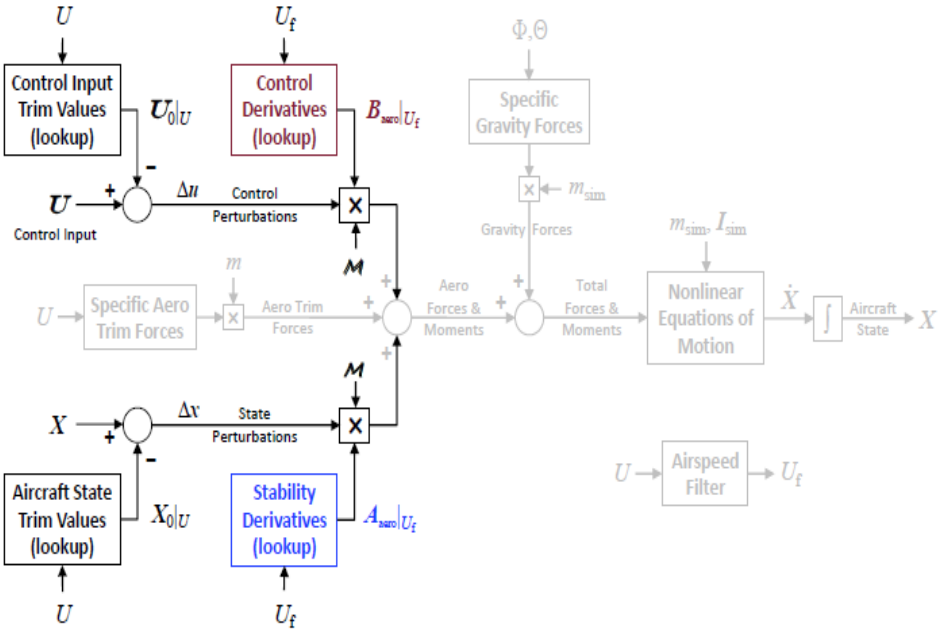

Figure 2 Model stitching simulation architecture - aero perturbation forces and moments

The specific aerodynamic/propulsion trim forces are calculated using the force balance in trim condition. Euler angles are tabulated with respect to discrete trim values. By using them, balancing trim gravitational forces could be found. Then, they are multiplied by the aircraft mass to obtain the dimensional aerodynamic/propulsion trim forces as shown in equation (11).

$$\begin{bmatrix} X_0 \\ Y_0 \\ Z_0 \end{bmatrix} = m \begin{bmatrix} \tilde{X}_0 \\ \tilde{Y}_0 \\ \tilde{Z}_0 \end{bmatrix} \quad (11)$$

This process of obtaining the dimensional aerodynamic trim forces is shown in Figure 3.

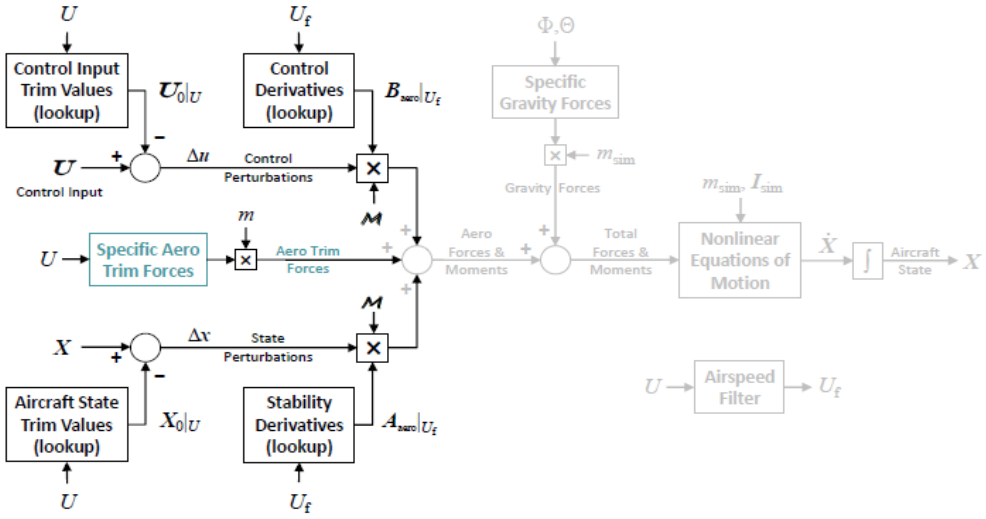

Figure 3 Model stitching simulation architecture – aerodynamic/propulsion trim forces

Calculation of the total dimensional aerodynamic/propulsive forces and moments combines the components covered thus far. The aerodynamic dimensional perturbation forces and moments [Equation (10)] are summed with the dimensional aerodynamic trim forces [Equation (11)] to yield the total aerodynamic/propulsive forces and moments. This summation is expressed in equation (12).

$$\{\vec{f_a}\}^{(B)} + \{\vec{f_p}\}^{(B)} = \begin{bmatrix} X \\ Y \\ Z \end{bmatrix} = \begin{bmatrix} X_0 \\ Y_0 \\ Z_0 \end{bmatrix} + \begin{bmatrix} \Delta X \\ \Delta Y \\ \Delta Z \end{bmatrix}$$
$$\{\vec{m}_B\}^{(B)} = \begin{bmatrix} l \\ m \\ n \end{bmatrix} = \begin{bmatrix} \Delta l \\ \Delta m \\ \Delta n \end{bmatrix} \quad (12)$$

and is shown graphically in Figure 4.

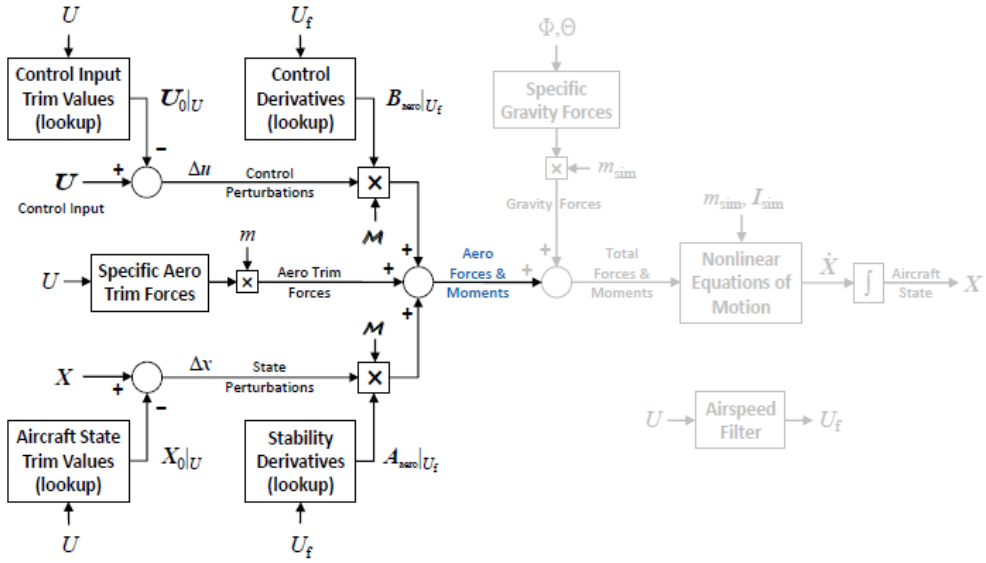

Figure 4 Model stitching simulation architecture - total aero forces and moments

The aerodynamic/propulsive forces and moments [Equation (12)] are summed with the gravity forces to yield the total external, dimensional forces and moments acting at the CM. This summation is expressed in equation (13).

$$\{\vec{f}\}^{(B)} = \left(\{\vec{f_a}\}^{(B)} + \{\vec{f_p}\}^{(B)}\right) + \{\vec{f_g}\}^{(B)} = \begin{bmatrix} X \\ Y \\ Z \end{bmatrix} + \begin{bmatrix} X_g \\ Y_g \\ Z_g \end{bmatrix} = \begin{bmatrix} X_0 \\ Y_0 \\ Z_0 \end{bmatrix} + \begin{bmatrix} \Delta X \\ \Delta Y \\ \Delta Z \end{bmatrix} + \begin{bmatrix} X_g \\ Y_g \\ Z_g \end{bmatrix}$$
$$\{\vec{m}_B\}^{(B)} = \begin{bmatrix} l \\ m \\ n \end{bmatrix} = \begin{bmatrix} \Delta l \\ \Delta m \\ \Delta n \end{bmatrix} \quad (13)$$

and is shown graphically in Figure 5.

Note that gravity force produces no external moment about the CM, so the total external moment is due to the total aerodynamic and propulsive moment alone.

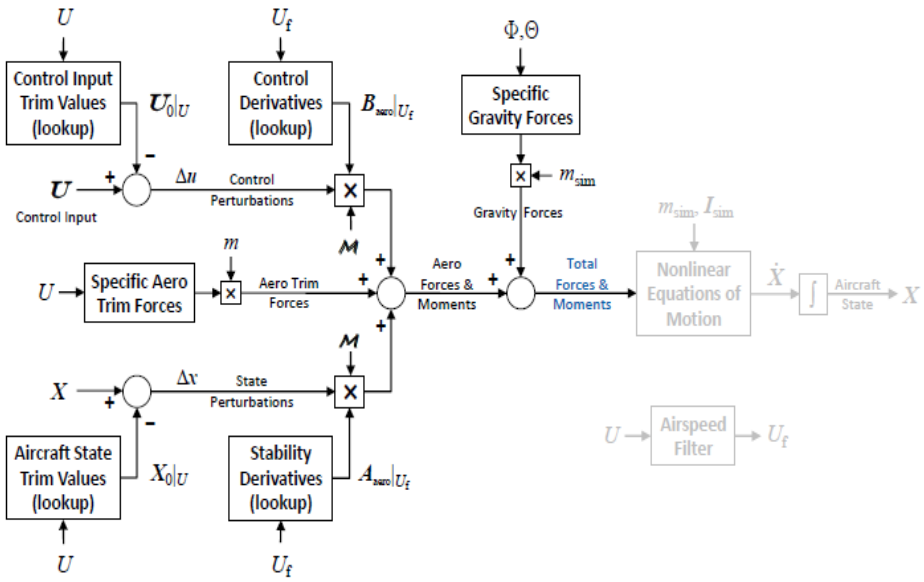

Figure 5 Model stitching simulation architecture - total forces and moments

Given total forces and moments about the aircraft CM, along with the current aircraft state and simulation values of mass and inertia, the 6-DOF body-axes nonlinear equation of motion is implemented to obtain the fuselage accelerations and Euler-angle rates. The equations of motion contain the nonlinear Euler equations, which include the cross-coupling inertial and Coriolis terms in full nonlinear form. The nonlinear equations of motion block is shown in Figure 6.

The force, moment and kinematic equations are combined together in equations (14).

$$\begin{aligned}
\dot{u} &= X/m - qw + rv - g\sin\theta \\
\dot{v} &= Y/m - ru + pw + g\cos\theta\sin\phi \\
\dot{w} &= Z/m - pv + qu + g\cos\theta\cos\phi \\
\dot{p} &= \frac{I_{XZ}(I_{XX} - I_{YY} + I_{ZZ})pq - (I_{ZZ}^2 - I_{YY}I_{ZZ} + I_{XZ}^2)qr + I_{ZZ}l + I_{XZ}n}{I_{XX}I_{ZZ} - I_{XZ}^2} \\
\dot{q} &= \frac{(I_{ZZ} - I_{XX})pr - I_{XZ}(p^2 - r^2) + m}{I_{YY}} \\
\dot{r} &= \frac{(I_{XX}^2 - I_{XX}I_{YY} + I_{XZ}^2)pq - I_{XZ}(I_{XX} - I_{YY} + I_{ZZ})qr + I_{XZ}l + I_{XX}n}{I_{XX}I_{ZZ} - I_{XZ}^2} \\
\dot{\phi} &= p + \mathrm{s}_\phi \mathrm{t}_\theta q + \mathrm{c}_\phi \mathrm{t}_\theta r \\
\dot{\theta} &= \mathrm{c}_\phi q - \mathrm{s}_\phi r \\
\dot{\psi} &= \mathrm{s}_\phi / \mathrm{c}_\theta q - \mathrm{c}_\phi / \mathrm{c}_\theta r
\end{aligned} \quad (14)$$

Total body-axes accelerations, body-axes angular rates and Euler-angle rates are collected to form the 6-DOF total state vector in equation (15).

$$\dot{\vec{x}} = [\dot{u} \quad \dot{v} \quad \dot{w} \quad \dot{p} \quad \dot{q} \quad \dot{r} \quad \dot{\phi} \quad \dot{\theta} \quad \dot{\psi}]^T \tag{15}$$

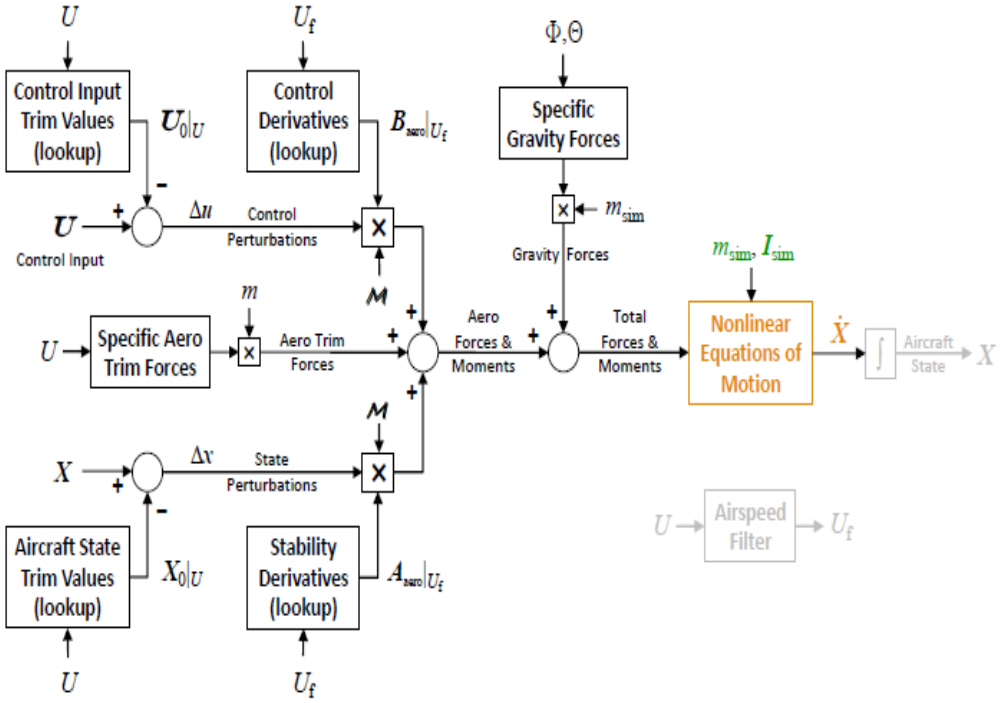

Figure 6 Model stitching simulation architecture - nonlinear equations of motion

The 6-DOF state-dot vector $\dot{\vec{x}}$, is comprised of the total body-axes accelerations, body-axes angular accelerations, and Euler-angle rates, is integrated forward in time to obtain the current 6-DOF aircraft state vector $\vec{x}$, given in equation (16).

$$\vec{x} = [u \quad v \quad w \quad p \quad q \quad r \quad \phi \quad \theta \quad \psi]^T \tag{16}$$

The integration routine in this study is Runge-Kutta 4 scheme and depicted in Figure 7 .

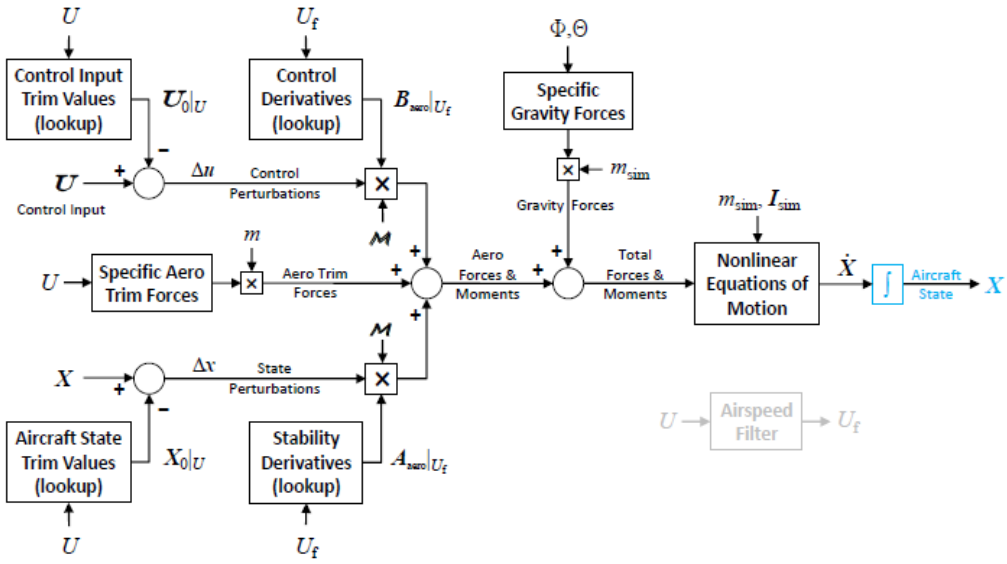

Figure 7 Model stitching simulation architecture - time integration

3. Model Evaluation Criteria

Analyses were performed for three model which are nonlinear model (shown as measured), stitching model and Jacobian Linearization model. Longitudinal and lateral motion will be presented separately. Elevator was used as an input in longitudinal motion whereas rudder and aileron were used as inputs in lateral motion. In longitudinal motion, phugoid and short period maneuvers were used to compare methods in order to show effectiveness in both fast and slow dynamics. In lateral motion, bank-to-bank and dutch roll maneuvers were used to compare methods for the same reason as in longitudinal motion. In order to compare the performance of the methods mentioned above, root of mean sum-of-squared errors is used and given in the equation (17).

$$RMSE = \sqrt{\frac{1}{n_{data}} \sum_{j=1}^{n_{data}} \left(z_j - y_j \right)^2} \tag{17}$$

j - the discrete data index

n_y - the number of neurons in the output layer.

n_{data} - the number of data

z_j^i - measured (actual) data in jth discrete data index

y_j^i - predicted data in jth discrete data index

RESULTS

1. Longitudinal Motion

1.1. Phugoid Mode

To show the effectiveness of methods, several analyses were performed with increasing input amplitude.

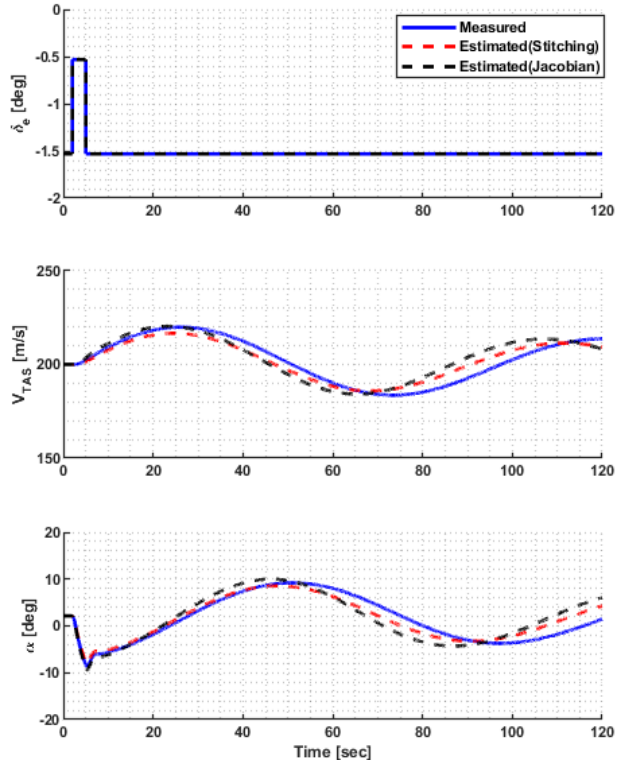

Figure 8 Phugoid simulation results with input amplitude is equal to 1

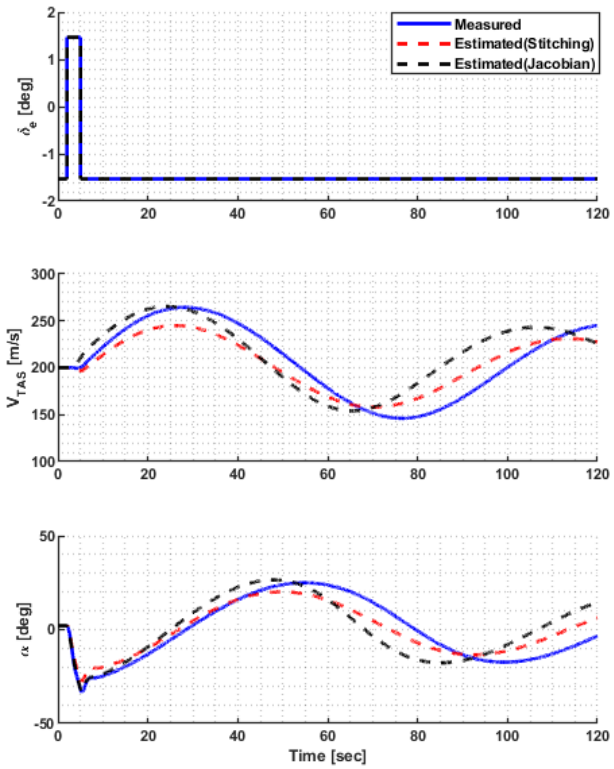

Figure 9 Phugoid simulation results with input amplitude is equal to 3

Simulation results are shown in Figure 8 and Figure 9 with different input amplitudes. Even though local models are obtained in the same trim points, results show that responses are different. It could be shown that, if number of local models are increased the response will be better. But this will result in longer computation time.

Results are compared with RMSE of each flight variable. With the increasing input amplitude, results get worse for both models. Even though, the model of “Model Stitching” results better in velocity than the model of “Jacobian Linearization”, the model of “Jacobian Linearization” results better in pitch angle.

Table 1 RMSE Evaluation of the phugiod maneuver result with different input amplitudes.

Models	$\Delta\delta_e = 1°$		$\Delta\delta_e = \mathbf{3}°$	
	V_{TAS}	θ	V_{TAS}	θ
Model Stitching	1.2486	0.5027	7.0185	4.1908
Jacobian Linearization	1.7129	0.4613	10.3222	1.1184

1.2. Short Period Mode

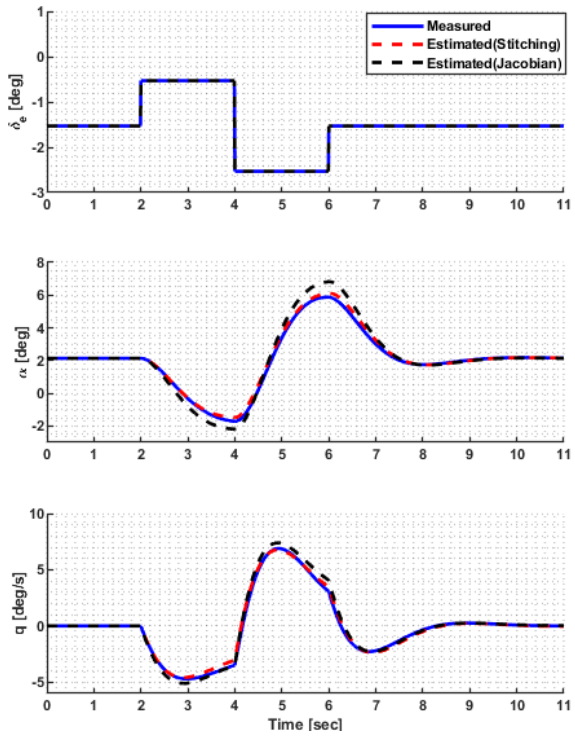

Figure 10 Short period simulation results with input amplitude is equal to 1

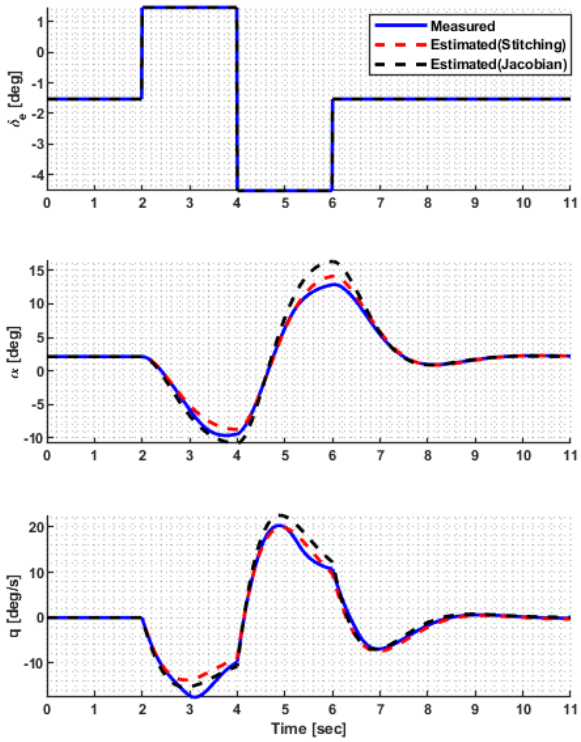

Figure 11 Short period simulation results with input amplitude is equal to 3

Simulation results are shown in Figure 10 and Figure 11 with input amplitudes of one and three, respectively. Even though it is shown clearly that the model of "Model Stitching" results more coherent than the model of "Jacobian Linearization", root mean squared errors of both are calculated as follows.

RMSE is calculated for both angle of attack and pitch rate. Results are shown in Table 2. As it can be seen, the model of "Model Stitching" results better than the model of "Jacobian Linearization" in both flight variables. With the increasing input amplitude, errors in results increase. And also, the gap between error of two models get bigger with increasing input amplitude.

Table 2 RMSE Evaluation of the short period maneuver result with different input amplitudes.

Models	$\Delta\delta_e = 1°$		$\Delta\delta_e = \mathbf{3}°$	
	α	q	α	q
Model Stitching	0.1245	0.1601	0.4313	1.0116
Jacobian Linearization	0.3361	0.2876	1.0069	1.1435

2. Lateral Motion

2.1. Bank-to-Bank Maneuver

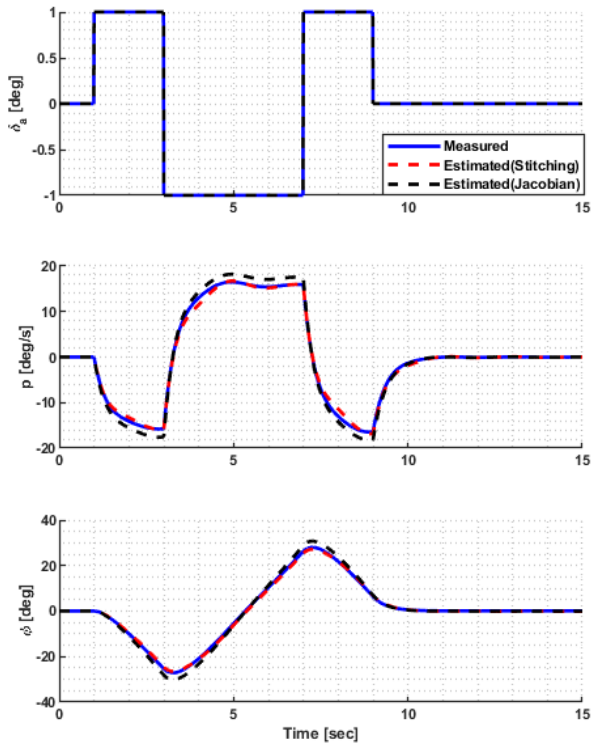

Figure 12 Bank-to-Bank simulation results with input amplitude is equal to 1

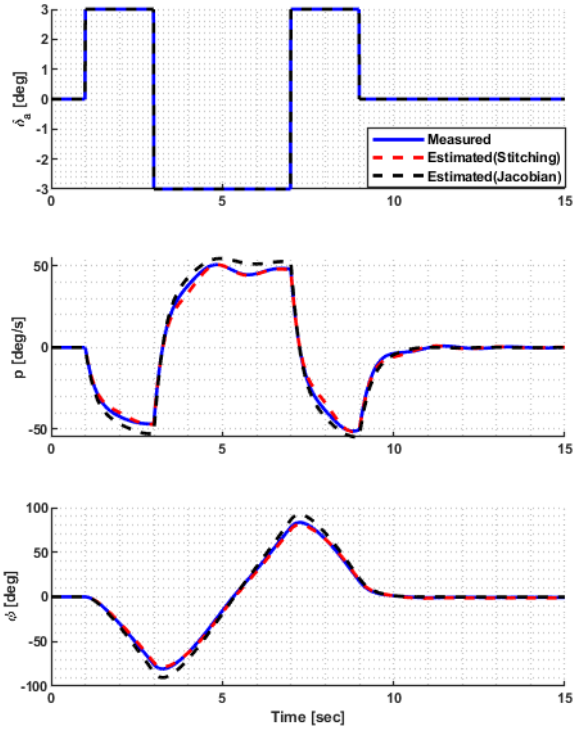

Figure 13 Bank-to-Bank simulation results with input amplitude is equal to 3

Simulation results are shown in Figure 12 and Figure 13 with input amplitudes of one and three, respectively.

Results are compared with RMSE of each flight variable in Table 3. With the increasing input amplitude, results get worse for both model. The model of “Model Stitching” results better than the model of “Jacobian Linearization” for both of the flight variables. As expected, gap between errors of two models get bigger with increasing input amplitude.

Table 3 RMSE Evaluation of the bank-to-bank maneuver result with different input amplitudes.

Models	$\Delta\delta_a = 1°$		$\Delta\delta_a = \mathbf{3}°$	
	p	ϕ	p	ϕ
Model Stitching	0.5407	0.4644	1.5777	1.3845
Jacobian Linearization	1.0531	1.3431	3.3102	4.3387

2.2. Dutch Roll Maneuver

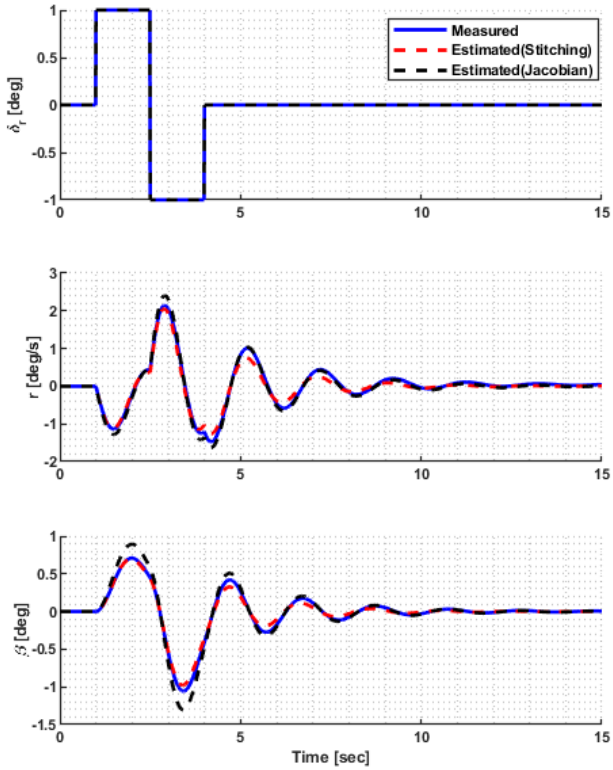

Figure 14 Dutch roll simulation results with input amplitude is equal to 1

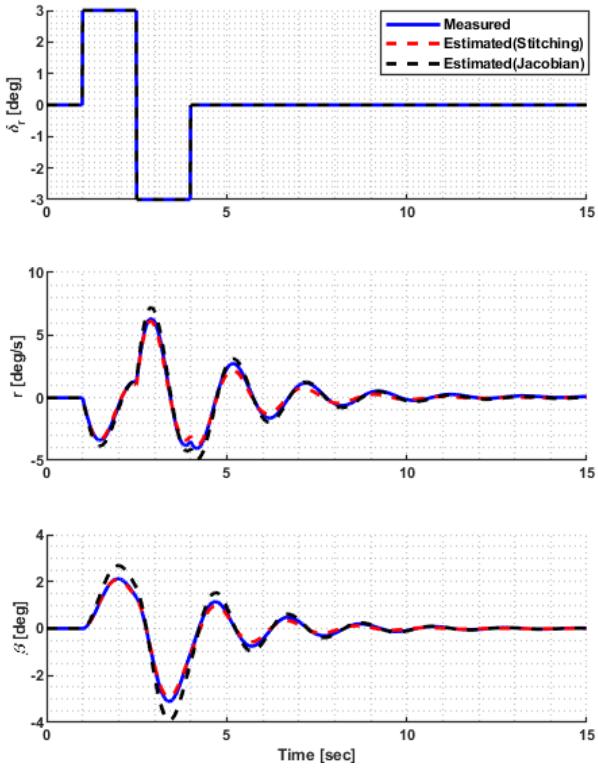

Figure 15 Dutch roll simulation results with input amplitude is equal to 3

Simulation results are shown in Figure 14 and Figure 15 with input amplitudes of one and three, respectively.

Results are compared with RMSE of each flight variable in Table 4. With the increasing input amplitude, results get worse for both model. When small input is applied on the systems, the model of "Jacobian Linearization" results better for yaw rate. But it is not valid when large input is applied on the system.

Table 4 RMSE Evaluation of the dutch-roll maneuver result with different input amplitudes.

Models	$\Delta\delta_r = 1°$		$\Delta\delta_r = \mathbf{3}°$	
	r	β	r	β
Model Stitching	0.1016	0.0367	0.2145	0.079
Jacobian Linearization	0.0738	0.0705	0.2723	0.2404

CONCLUSION

Model was analyzed with phugoid, short period, bank-to-bank and Dutch roll maneuvers separately. It is shown that, even though models' responses are closely matched by using small inputs, Jacobian Linearization model respond divergently by large inputs as expected, except for phugoid maneuver. It is evaluated that the exception comes from slow dynamics. Slow dynamic allows Jacobian Linearization to be more coherent with nonlinear model than Model Stitching.

Results are compared with calculated RMSE of results. It is shown that with increasing input amplitude, errors increase for both LPV models. It would be overcome by increasing number of local models. But this will result in more computational times.

Results show that Model Stitching outperforms Jacobian Linearization if number of local models are the same. Even though Jacobian Linearization is easier to model, it cannot get better results especially in large inputs. Jacobian Linearization would be used with increasing number of local models in order to get better results.

References

[1] Marcos and G. Balas, "Linear Parameter Varying Modeling of the Boeing 747-100/200 Longitudinal Motion," in AIAA Guidance, Navigation, and Control, Montreal, 2001.

[2] M. Millidere, U. Karaman, S. Uslu, C. Kasnakoglu and T. Çimen, "Newton Raphson Methods in Aircraft Trim: A Comparative Study," in AIAA Aviation Forum, Reno, NV, 2020.

[3] A. Marcos and G. Balas, "Development of Linear-Parameter-Varying Models for Aircraft," Journal of Guidance, Control, and Dynamics, vol. 27, no. 2, 2004.

[4] M. B. Tischler and E. L. Tobias, "A Model Stitching Architecture for Continuous Full Flight-Envelope Simulation of Fixed-Wing Aircraft and Rotorcraft from Discrete Point Linear Models," U.S. Army Research, Development, and Engineering Command, 2016.

[5] S. Armanini, M. Karasek and C. de Visser, "Global LPV model identification of flapping-wing dynamics using flight data," in AIAA Modeling and Simulation Technologies Conference, Kissimmee, FL, 2018.

[6] L. Nguyen, M. Ogburn, W. P. Gilbert, K. S. Kibler, P. W. Brown and P. L. Deal, "Simulator Study of Stall/PostStall Characteristics of a Fighter Airplane with Relaxed Longitudinal Static Stability," NASA Technical Paper 1538, Hampton, VA, 1979.

[7] Smaili, M.H., “FLIGHTLAB 747: Benchmark for Advanced Flight Control Engineering,” Tech. rep., Technical University Delft, The Netherlands, 1999